Applied Catalysis B: Environmental 214 (2017) 15–22

Contents lists available at ScienceDirect

Applied Catalysis B: Environmental

journal homepage: www.elsevier.com/locate/apcatb

Research paper

Size-dependent plasmonic effects of M and M@SiO_2 (M = Au or Ag) deposited on TiO_2 in photocatalytic oxidation reactions

Ji Eun Lee, Sandipan Bera, Young Sik Choi, Wan In Lee*

Department of Chemistry and Chemical Engineering, Inha University, Incheon 402-751, Korea

ARTICLE INFO

Article history:
Received 8 April 2017
Received in revised form 1 May 2017
Accepted 7 May 2017
Available online 9 May 2017

Keywords:
Plasmonic photocatalyst
Photocatalytic oxidation reaction
LSPR effect
Au and Ag nanoparticle
Au@SiO_2 and Ag@SiO_2

ABSTRACT

Monodispersed Au nanoparticles (NPs) with sizes of 18, 26 and 34 nm and Ag NPs with sizes of 17, 25 and 33 nm, as well as their corresponding M@SiO_2 core-shell NPs (M = Au or Ag), were selectively synthesized. The prepared individual plasmonic NPs were then loaded onto TiO_2 and their size-dependent plasmonic effects in photocatalytic oxidation reactions were systematically analyzed. In the removal reactions of the organic compounds, aqueous salicylic acid (SA) and aniline, under UV–vis light irradiation, both the Au and Ag NPs significantly enhanced the catalytic activity of TiO_2, while the smaller NPs were more effective. Although the Ag NPs show stronger LSPR effect than the Au NPs, the overall catalytic activity of the Ag/TiO_2 systems was not higher than Au/TiO_2, and their catalytic activity variation according to the size of plasmonic NPs was more sensitive for Ag/TiO_2. The observed results seem to be due to the LSPR sensitization effect. It was also found that the M@SiO_2 NPs were significantly more effective than the bare M NPs in enhancing the photocatalytic activity of TiO_2 and the size-dependent plasmonic effects of the M@SiO_2 NPs were quite different from those of the bare M NPs. In regrading to catalytic activity enhancement, the optimum sizes of the Au and Ag NPs for the Au@SiO_2 and Ag@SiO_2 NPs were determined to be 26 and 25 nm, respectively. Moreover, the Ag@SiO_2 NPs, which generate stronger LSPR, were more effective than the Au@SiO_2 NPs. Consequently, Ag25@SiO_2/TiO_2 demonstrates the highest activity in decomposing SA and aniline, which is 3.8 and 2.5 times, respectively, that of the bare TiO_2.

1. Introduction

Photocatalytic degradation of organic pollutants has been extensively investigated as one of the most promising green technologies, since Honda and Fujishima reported the photocatalytic properties of TiO_2 in 1972 [1]. Presently, TiO_2 in the anatase phase with a band gap of 3.2 eV is known as the most effective photocatalyst, but its catalytic efficiency needs to be further improved for commercial applications.

A promising strategy for enhancing the photocatalytic efficiency of TiO_2 is to load noble metals on its surface [2–11]. Thus far, various noble metals such as Au [3,4], Ag [5,6], Cu [7], Pt [8,9], Pd [10] and others [8,11] have been employed, and many reports indicated that the photocatalytic activity of TiO_2 can be significantly enhanced by loading these noble metals. Conventionally, the major role of the metals deposited on the TiO_2 surface was regarded to be the promotion of charge-separation by forming a Schottky junction [12,13]. Considering that the Fermi levels of most noble metals are located below the conduction band (CB) of TiO_2, the electrons in the TiO_2 CB by excited UV light irradiation will be transferred spontaneously to the loaded noble metals. Thus the charge recombination taking place in the TiO_2 will be suppressed, and the holes in the TiO_2 valence band (VB) will then have a longer lifetime, which facilitates the participation of the holes in oxidation reactions [12–16].

Recently, however, many reports indicated that the plasmonic effect of noble metals plays a more important role in enhancing the photocatalytic activities for noble metal loaded TiO_2 systems [2,17–19]. Nano-sized noble metals such as Au and Ag generate intense localized surface plasmonic resonance (LSPR) by absorbing photons in the wavelength corresponding to their plasmonic absorption bands. Thus, the strongly enhanced electric field generated in the plasmonic nanoparticles (NPs) can stimulate bandgap excitation for the TiO_2 particles in their vicinity. As a result, the photocatalytic activity can be increased due to the generation of more electron-hole pairs in the TiO_2 [20–23]. In addition to the local electric field enhancement, several other effects also accompany the LSPR effect. That is, 'local heating effect', 'LSPR sensitization effect' and others can take place at the same time, as shown in Scheme 1a. Upon irradiation by visible-light corresponding to their plasmonic absorption band, local heat can be generated due to the fast oscilla-

* Corresponding author.
E-mail address: wanin@inha.ac.kr (W.I. Lee).

http://dx.doi.org/10.1016/j.apcatb.2017.05.025
0926-3373/

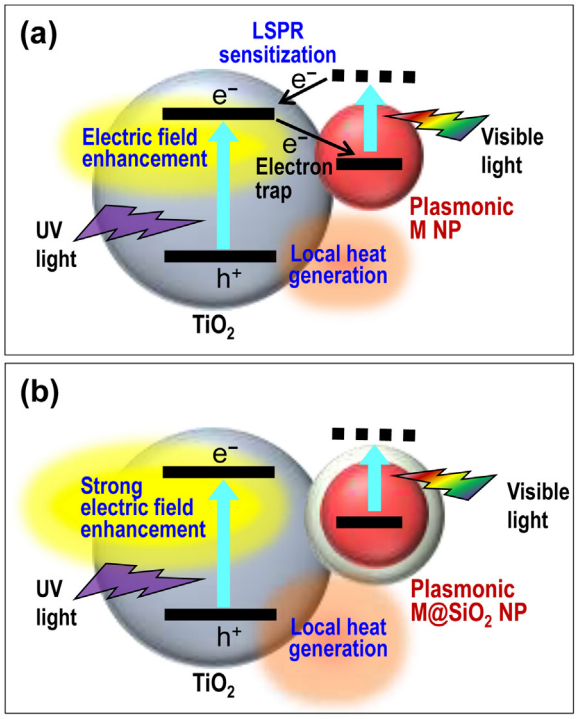

Scheme 1. Schematic diagram for the plasmonic effects occurring in the noble metal (M = Au and Ag) NPs (a) and M@SiO_2 NPs (b) deposited on TiO_2 under UV–vis light irradiation. Individual plasmonic effects are indicated in blue ink. (For interpretation of the references to colour in this figure legend, the reader is referred to the web version of this article.)

tion of electrons along the plasmonic NPs. Significant temperature elevations were monitored by irradiating high-intensity laser light onto the plasmonic NPs, but under the irradiation of light of about one sun intensity, the amount of local heat generated is not significant [23–26].

Another noticeable effect is the 'LSPR sensitization effect' [23]. Under visible light irradiation, the electrons in the noble metals can be excited by LSPR, and then fed into the CB of TiO_2. As a result, the electrons transported to the TiO_2 CB can induce various reduction or oxidation reactions [27–29], whereas the holes generated in the plasmonic NPs can participate in oxidation reactions. However, only mild or partial oxidation reactions can take place, because the holes in the noble metal NPs do not have strong oxidative power. Recently, there have been various reports on the selective oxidation reactions induced by Au/TiO_2 under visible light irradiation [27–32]. Under UV–vis irradiation, however, the contribution in catalytic reactions by the holes in the noble metal NPs will not be significant for the noble metal loaded TiO_2 systems, because the holes generated by the band gap excitation of TiO_2 exhibit much stronger oxidation power. Furthermore, under UV–vis light condition, the 'LSPR sensitization effect' may not be beneficial to the photocatalytic oxidation reactions. In effect, there is a high possibility that the excitation from the noble metal to the TiO_2 CB prevents the space-charge separation of the electron-hole pairs in TiO_2 generated by bandgap excitation because the electrons transported to the noble metal NPs can go back to the TiO_2 CB, as seen in Scheme 1a.

It is known that the LSPR effect of plasmonic NPs is strongly dependent on their particle size. As the size of the metal NPs increases, higher electric field is induced in the vicinity of the plasmonic NPs due to the increase of the LSPR strength [33–49]. It has also been reported that covering the noble metals with dielectric materials such as SiO_2 can further enhance the LSPR [4,37–41]. Moreover, in contrast to the bare noble metal NPs, the silica-covered noble metal (M@SiO_2) NPs show much different behavior, when M@SiO_2 NPs are loaded on the TiO_2 surface, as shown in Scheme 1b. Due to the presence of a dielectric layer over the noble metal, the electrons generated in the TiO_2 CB cannot be trapped by the noble metal, and also the excited electrons in the noble metals cannot be transferred to the TiO_2 CB. Therefore, in the M@SiO_2/TiO_2 system, the enhancement of the local electric field is considered to be the major factor expediting photocatalytic reactions.

Previously, we prepared several types of Au NPs with the sizes of 3, 7 and 17 nm, as well as their corresponding Au@SiO_2 core-shell structures, and analyzed the size dependent plasmonic effect for the photocatalytic Au/TiO_2 and Au@SiO_2/TiO_2 systems [30]. In decomposing aqueous salicylic acid (SA) under UV–vis light irradiation, the 3 nm-sized Au NP loaded TiO_2 (Au3/TiO_2) showed the highest efficiency among the Au/TiO_2 systems, suggesting that the charge-separation effect is the dominant factor. Contrarily, among the Au@SiO_2 NPs, the Au17@SiO_2 (17 nm-sized Au NPs covered by SiO_2 shell) loaded TiO_2 showed the highest efficiency.

In this work, we prepared relatively larger Au NPs and their corresponding Au@SiO_2 core-shell structures to complete the analysis of the size-dependent plasmonic effect. To evaluate the photocatalytic activities of the TiO_2 loaded with plasmonic NPs, aniline, a basic compound, was also applied as a model compound in addition to SA. Furthermore, we prepared various Ag NPs and their corresponding Ag@SiO_2 NPs. It is known that Ag NPs exhibit stronger LSPR than Au NPs [50,51]. Thus, the analysis of the size effects for Ag and Ag@SiO_2 NPs is expected to provide key information to facilitate our understanding on the plasmonic effects in photocatalytic oxidation reactions. Also, we successfully determined the optimum sizes for the plasmonic NPs based on Au and Ag. The results obtained will guide us to design highly efficient plasmonic photocatalysts.

2. Experimental

2.1. Syntheses of materials

2.1.1. Synthesis of Au NPs

18, 26 and 34 nm-sized Au NPs (termed as Au18, Au26 and Au34, respectively) were prepared using a citrate reduction method by varying the ratio of sodium citrate to $HAuCl_4$ [52–54]. While 95 ml of 0.25 mM $HAuCl_4$ aqueous solution in a flask was refluxed at 110 °C, 43 mg of sodium citrate in 10 ml of H_2O was added to prepare Au18, whereas 17 mg and 10 mg of sodium citrate in 10 ml H_2O were added to obtain Au26 and Au34, respectively. The mixture was then refluxed for an additional 30 min. The color of the solution changed from pale pink to a deep red when the reaction was finished. The prepared Au NPs were collected by centrifugation and washed with water several times.

2.1.2. Synthesis of Au@SiO_2 NPs

Silica was coated on the surfaces of the Au NPs by a modified Stöber process [55,56]. Composition of the silica solution for the coverage of the Au NPs was varied according to the size of the Au NPs. That is, for the coverage of Au18, 8.3 μl tetraethyl orthosilicate (TEOS), 53.4 ml ethanol, 2 ml H_2O and 0.80 ml NH_4OH (28–30% in water, Aldrich) were mixed and vigorously stirred for 30 min. Then, 3 mg Au18 NPs suspended in 2 ml H_2O was added to this silica solution, and the mixture was stirred vigorously for 6 h under ambient condition. The prepared Au18@SiO_2 NPs were then collected by centrifugation and washed with ethanol. For the preparation of Au26@SiO_2, the composition of the silica stock solution was 37.8 ml ethanol, 1.42 ml H_2O, 0.57 ml NH_4OH and 6.3 μl TEOS, whereas that of the silica solution for Au34@SiO_2 was 25.8 ml ethanol, 0.97 ml H_2O, 0.39 ml NH_4OH, and 4.3 μl TEOS.

To prepare the 25 nm-sized SiO_2 NPs, 100 ml methanol, 3.5 ml NH_4OH and 9 ml water were pre-mixed. 6.25 ml TEOS was then added and the mixture was vigorously stirred for 1 h under ambient condition. The prepared SiO_2 NPs were collected by centrifugation at 20,000 rpm for 1 h, and washed with isopropyl alcohol several times.

2.1.3. Synthesis of Ag NPs

The 17 nm-sized Ag NPs (Ag17) were prepared by a polyol method [57,58]. 0.5 g of polyvinylpyrrolidone (PVP-10) was dissolved in 25 ml ethylene glycol at room temperature, and then 17 mg of $AgNO_3$ was added to this solution. The suspension was stirred at room temperature until the silver nitrate was completely dissolved. Then, the solution was slowly heated up to 120 °C and kept at this temperature for 1 h. After cooling down the suspension, the Ag NPs were collected by centrifugation and washed with acetone and ethanol several times. The 25 and 33 nm-sized Ag NPs (Ag25 and Ag33, respectively) were prepared by a modified citrate reduction method by varying the ratio of tannic acid to sodium citrate [58]. For the preparation of the Ag25 NPs, 100 ml of 5 mM sodium citrate aqueous solution was mixed with 0.01 mmol tannic acid. When the reaction mixture was heated up to 120 °C, 1 ml of 25 mM $AgNO_3$ was added and kept for additional 1 h at this temperature. The prepared Ag NPs were collected by centrifugation and washed with water several times to remove the remaining reductants. For the preparation of Ag33 NP, 0.025 mmol tannic acid was employed, while the other conditions were kept the same.

2.1.4. Synthesis of Ag@SiO_2 NPs

To coat silica on the surface of the Ag17 NPs, a modified Stöber process was applied [55,60]. Initially, 53.4 ml ethanol, 2 ml H_2O, 0.80 ml NH_4OH (28–30% in water, Aldrich) and 8.3 μl tetraethyl orthosilicate (TEOS) were mixed and stirred vigorously for 30 min. Three mg of Ag17 in 2 ml H_2O was then added to this solution, and the mixture was vigorously stirred for 6 h under ambient condition. The prepared Ag17@SiO_2 NPs were then collected by centrifugation and washed with ethanol.

For the preparation of Ag25@SiO_2 and Ag33@SiO_2, an ammonia-free synthetic route was utilized to avoid the partial dissolution of Ag NPs by NH_4OH during the silica coating process [61]. Four μL TEOS was dissolved in 20 ml ethanol and, subsequently, 3 mg Ag NPs (Ag25 or Ag33) in 2 ml water and 0.25 ml of 40% dimethylamine (Aldrich) were added, followed by vigorous stirring for 20 h. The prepared Ag@SiO_2 NPs were centrifuged and washed with ethanol several times.

2.1.5. Preparation of M/TiO_2 and M@SiO_2/TiO_2

One gram TiO_2 powder (Degussa P25) and 0.01 g maleic acid were suspended in 20 ml ethanol and stirred at 500 rpm. Three mg metal NPs (M NPs) or silica coated metal NPs (M@SiO_2 NPs) were suspended in 5 ml ethanol, regardless of the size of the NPs. Then, to prepare the M/TiO_2 and M@SiO_2/TiO_2 with different percentages (0.3–0.6 wt%), stoichiometric amounts of the M NPs or M@SiO_2 NPs solution were slowly added to the TiO_2 suspension and the resultant suspensions were refluxed for 12 h while stirring at 500 rpm. The precipitate was collected by centrifugation at 6000 rpm, washed three times with ethanol, and finally dried in a vacuum. To remove remaining organics, each catalytic sample was irradiated with a 300 W Xe-lamp (Oriol) for 3 h.

2.2. Characterization

Field emission transmission electron microscopy (FE-TEM) images were obtained by a JEOL JEM2100F operated at 200 kV. One milligram of the synthesized particles was dispersed in 50 ml of ethanol, and a drop of the suspension was then spread on a holey amorphous carbon film deposited on the copper grid. UV–vis absorbance spectra were acquired using a Perkin-Elmer Lambda 40 spectrophotometer.

2.3. Evaluation of photocatalytic activity

For the evaluation of photocatalytic activities of various plasmonic photocatalysts, salicylic acid (SA) and aniline were used as model compounds. SA and aniline aqueous solutions are not volatile under ambient condition and their concentrations can be easily determined from their characteristic absorption peak at 295 nm and 230 nm, respectively. The total volume of the solution for the photocatalytic reaction was 60 ml, the concentration of SA or aniline was 1.50×10^{-4} M, and 10 mg of photocatalytic sample was suspended in this solution. While stirring, the solution in a quartz reactor was irradiated by the light sources. As the UV–vis source, a 300 W Xe lamp (Oriel) was used in conjunction with a water filter to cut-off IR. Wavelength range of the light source was 300–900 nm, while its intensity was 5 W/cm^2. Second, to obtain UV light, a visible light cutoff filter (λ > 400 nm, Asahi Inc.) was additionally installed on the 300 W Xe lamp. After every 30 min of irradiation, the remnant concentration of SA (or aniline) in the solution was analyzed based on its characteristic absorption peak with a UV–vis spectrophotometer (Perkin-Elmer Lambda 40).

Since the removal of the aqueous SA approximates the first order kinetics, the photocatalytic decomposition reaction can be described by $-d[c]/dt = k[c]$, where $[c]$ is the concentration of SA, and k denotes the degradation rate constant. The determined k value was defined as the photocatalytic activity of each sample.

3. Results and discussion

As seen in the TEM images in Fig. 1a–c, the as-prepared Au NPs exhibit monodispersed spherical or oval morphologies with average diameters of 18, 26, and 34 nm, respectively. Employing these Au NPs, Au@SiO_2 core–shell structures were prepared by a sol–gel process [52–56]. The TEM images of Fig. 1d–f indicate that the SiO_2 shell thicknesses of the Au@SiO_2 core-shell structures are about 10 nm for all of the Au NPs. Similarly, Ag NPs with average diameters of 17, 25, and 33 nm were also prepared, as shown in Fig. 2a–c. Employing these Ag NPs, Ag@SiO_2 core-shell structures were also synthesized by several sol–gel processes [57–61]. TEM images of Fig. 2d–f indicate that the SiO_2 shell thicknesses of the Ag@SiO_2 core–shell structures are ~10 nm for all of the Ag NPs.

It is reported that LSPR effect of M@SiO_2 is strongly dependent on the SiO_2 shell thickness [6,62–64]. For instance, several researchers investigated the intensity enhancement of photoluminescence (PL) for the fluorescent dyes anchored on the Ag@SiO_2 core-shell structures with various SiO_2 shell thicknesses. They observed that PL enhancement was maximized by introducing ~8 nm-thick SiO_2 shell [62,63]. In addition, the effect of SiO_2 shell thickness in the photocatalytic activities of spherical SiO_2/Ag/SiO_2/TiO_2 systems was investigated, but the photocatalytic systems were quite different from ours. They reported that the optimum SiO_2 shell thickness is about ~5 nm [6,64]. From our preliminary work, the optimum thickness of SiO_2 shell for the Ag@SiO_2 NPs, in regarding to the photocatalytic activity enhancement of TiO_2 by plasmonic effect, was ~8 nm, but the activity enhancement was not appreciably changed for the SiO_2 layers in the range of 6–10 nm. In order to analyze the size-dependent plasmonic effect of Au and Ag NPs, the shell thickness of SiO_2 layer must to be kept the same. Hence, we fixed the shell thickness as 10 nm, which is easier to control and more reproducible in preparation.

UV–vis absorption spectra of the various Au and Au@SiO_2 NPs suspended in aqueous solution are shown in Fig. 3a. The

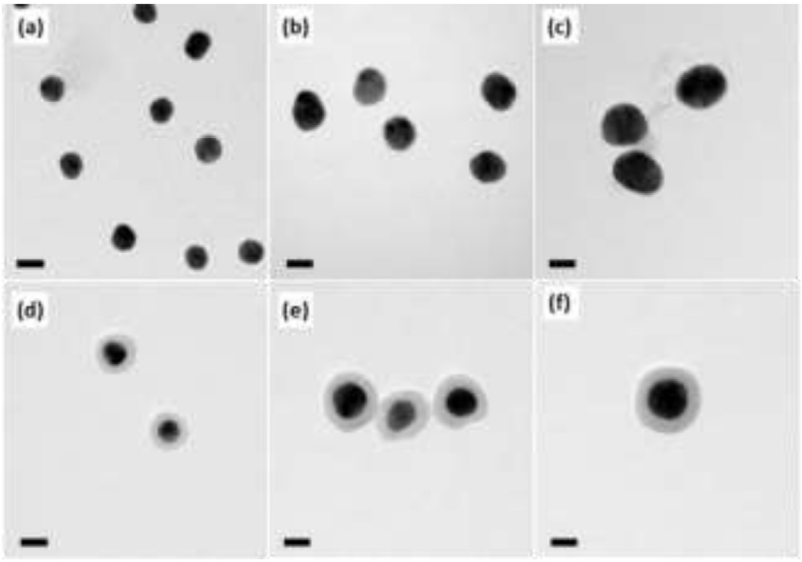

Fig. 1. TEM images of Au18 (a), Au26 (b), Au34 (c), Au18@SiO_2 (d), Au26@SiO_2 (e) and Au34@SiO_2 (f). All of the scale bars indicate 20 nm.

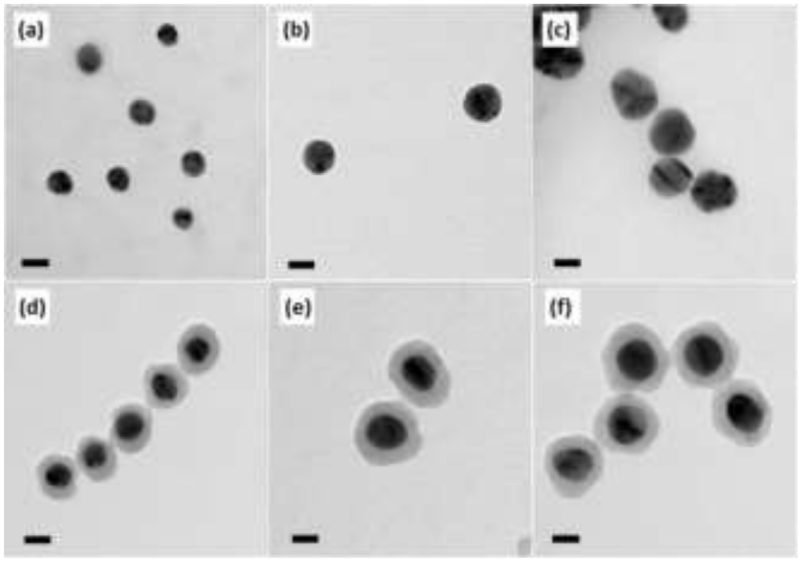

Fig. 2. TEM images of Ag17 (a), Ag25 (b), Ag33 (c), Ag17@SiO_2 (d), Ag25@SiO_2 (e) and Ag33@SiO_2 (f). All of the scale bars indicate 20 nm.

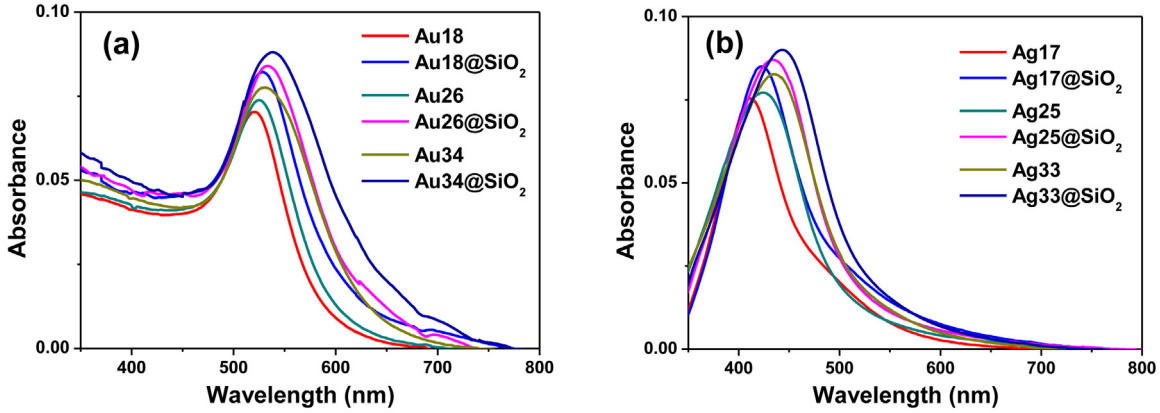

Fig. 3. UV–vis absorption spectra of various Au and Au@SiO_2 NPs (a), and Ag and Ag@SiO_2 NPs (b) suspended in aqueous solution. In the Au@SiO_2 and Ag@SiO_2 NPs, the SiO_2 shell thicknesses were controlled to ~10 nm.

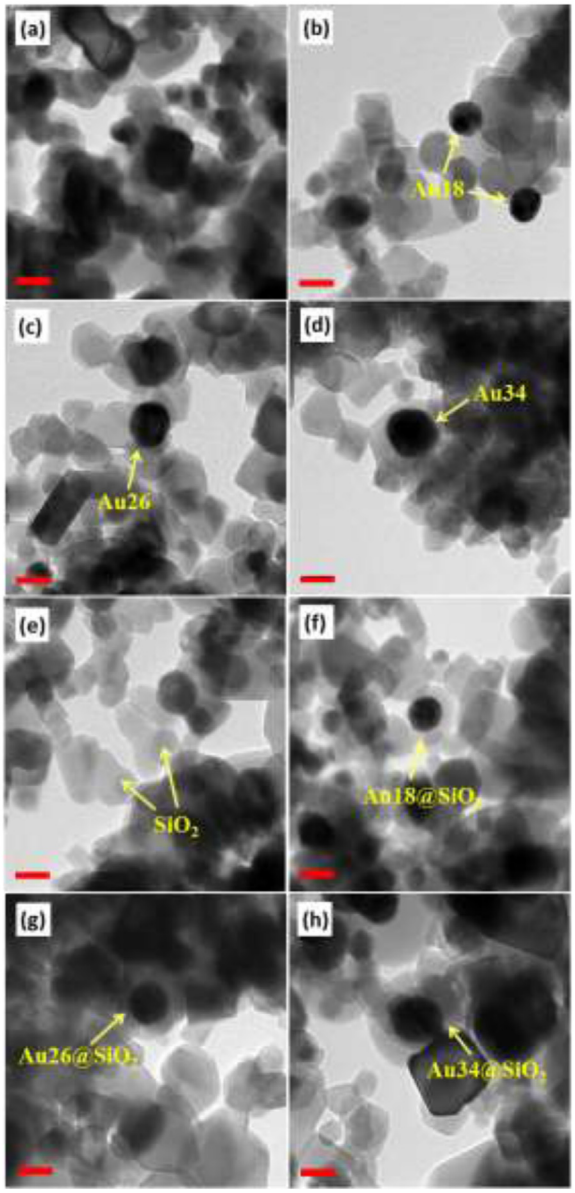

Fig. 4. TEM images of bare TiO_2 (a), Au18/TiO_2 (b), Au26/TiO_2 (c), Au34/TiO_2 (d), bare SiO_2/TiO_2 (e), Au18@SiO_2/TiO_2 (f), Au26@SiO_2/TiO_2 (g) and Au34@SiO_2/TiO_2 (h). All of the scale bars indicate 20 nm.

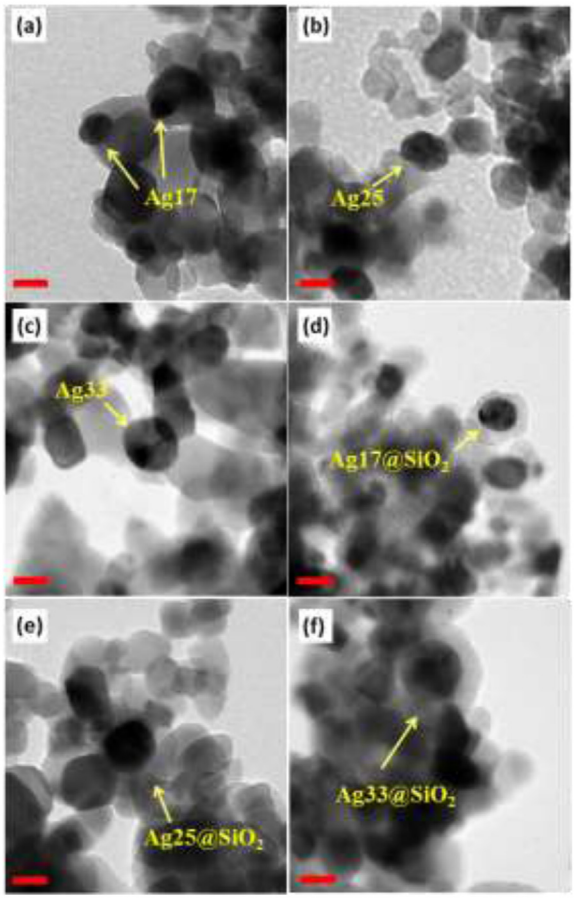

Fig. 5. TEM images of Ag17/TiO_2 (a), Ag25/TiO_2 (b), Ag33/TiO_2 (c), Ag17@SiO_2/TiO_2 (d), Ag25@SiO_2/TiO_2 (e) and Ag33@SiO_2/TiO_2 (f). All of the scale bars indicate 20 nm.

18 nm-sized Au NP (Au18) reveals plasmonic absorption maxima at 520 nm, and its peak position is slightly red-shifted, as the size of the Au NPs increases. Also, the coverage of silica induces a shift of the plasmonic absorption peak to a longer wavelength, which is in good agreement with the reports in the literature [23,24,38]. UV–vis absorption spectra of the Ag and Ag@SiO_2 NPs suspended in aqueous solution, as seen in Fig. 3b, indicates that the 17 nm-sized Ag NP (Ag17) shows the plasmonic absorption maxima at 412 nm, and the peak position is gradually red-shifted, as the size of the Ag NPs increases. Also, the introduction of the SiO_2 shell induces an appreciable shift of the plasmonic absorption peak toward a longer wavelength.

In preparing the plasmonic photocatalysts, each of the Au, Ag, Au@SiO_2 and Ag@SiO_2 NP was deposited onto TiO_2 (Degussa P25) by utilizing maleic acid as an anchoring agent. TEM images of the bare TiO_2 (Degussa P25), Au18-loaded TiO_2 (Au18/TiO_2), Au26/TiO_2, and Au34/TiO_2, in Fig. 4a–d, show the Au NPs sparsely appearing around the agglomerated TiO_2 particles. In these samples, the amounts of the loaded Au NPs relative to TiO_2 were 0.5, 0.6 and 0.6 wt%, respectively. Fig. 4e–h show TEM images of the bare SiO_2/TiO_2, Au18@SiO_2/TiO_2, Au26@SiO_2/TiO_2, and Au34@SiO_2/TiO_2, respectively, exhibiting the presence of Au@SiO_2 NPs on the agglomerated TiO_2 particles. Fig. 5a–c show TEM images of Ag17-loaded TiO_2 (Ag17/TiO_2), Ag25/TiO_2, and Ag33/TiO_2, respectively. The composition of Ag NPs relative to TiO_2 was 0.5 wt% for all of the Ag/TiO_2 and Ag@SiO_2/TiO_2 samples. Fig. 5d–f show TEM images of the Ag17@SiO_2/TiO_2, Ag25@SiO_2/TiO_2, and Ag33@SiO_2/TiO_2, respectively, showing the Ag@SiO_2 NPs present on the agglomerated TiO_2 particles.

In order to investigate the size dependent plasmonic effects of the Au, Au@SiO_2, Ag, and Ag@SiO_2 NPs in photocatalytic oxidation reactions of TiO_2, two kinds of light sources were employed in this work. First, a 300 W Xe-lamp in conjunction with visible light ($\lambda > 400$ nm) and IR ($\lambda > 800$ nm) cut-off filters was applied as UV light source. The irradiated photons in this UV region are suitable for the bandgap excitation of TiO_2, but will not be efficient for the activation of plasmonic NPs. Second, as UV–vis light source, 300 W Xe-lamp in conjunction with only an IR cut-off filter was applied. With the irradiation of UV–vis light, in addition to the bandgap excitation of TiO_2, the loaded Au- and Ag-based plasmonic NPs can be activated to generate the characteristic LSPR effect.

The influence of the plasmonic effect afforded by the Au, Au@SiO_2, Ag, and Ag@SiO_2 NPs on the photocatalytic activity of TiO_2 will be dependent on their loading concentrations. Thus, the optimum concentration of the individual plasmonic NPs has to be determined for the reasonable estimation and comparison of plasmonic effects. Herein, the decomposition rates of SA in aqueous solution under UV–vis light were monitored as a function of

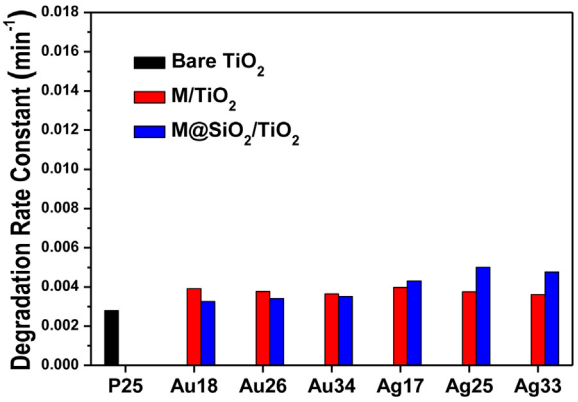

Fig. 6. Bar graphs for the degradation rate constants (k) of the bare TiO_2 and various plasmonic photocatalysts in decomposing aqueous SA under UV light.

plasmonic NP concentration in the plasmonic photocatalysts. As shown in Fig. S1, the optimum concentrations of Au18, Au26, and Au34 for the Au/TiO_2 systems were determined to be 0.5, 0.6, and 0.6 wt%, respectively, whereas those of the Ag NPs for the Ag/TiO_2 systems are determined to be 0.5 wt%, regardless of the size of NPs, as seen in Fig. S2. The optimized concentrations of the individual plasmonic NPs were then employed to prepare various Au/TiO_2, $Au@SiO_2/TiO_2$, Ag/TiO_2 and $Ag@SiO_2/TiO_2$ samples in order to analyze their size-dependent LSPR effects in the photocatalytic oxidation reactions.

First of all, photocatalytic activities of the various plasmonic photocatalysts were evaluated under UV light irradiation. The degradation rate constants (k) of SA obtained from the various plasmonic photocatalysts are summarized in Fig. 6, while the decomposition rates as a function of irradiation time for the individual plasmonic photocatalysts are illustrated in Fig. S3. The Au/TiO_2 and $Au@SiO_2/TiO_2$ samples showed higher catalytic activities than the bare TiO_2, although the degree of enhancements was not high. In addition, the Au/TiO_2 samples showed relatively higher catalytic activities than the $Au@SiO_2/TiO_2$ systems. As is well known, the two major roles of the noble metals in increasing the photocatalytic activity of TiO_2 are (1) promotion of charge-separation by forming a Schottky junction [12,13] and (2) enhancement of the local electric field through its LSPR effect. It was also reported that the LSPR effect can be enhanced by increasing the size of the plasmonic NPs [33–49] or covering them with dielectric materials such as silica [37–41]. Under UV light irradiation, the LSPR effect will not be significant because Au NPs are not efficiently activated by the photons in the UV region, considering that their plasmonic absorption bands are in the range of 500–600 nm, as shown in Fig. 3a. Therefore, the increase of catalytic activity for the Au/TiO_2 samples can be mainly attributed to the charge-separation role of the Au NPs. In contrast, for the $Au@SiO_2/TiO_2$ samples, the presence of the dielectric SiO_2 layer with a thickness of ~10 nm blocks the charge transport from the TiO_2 CB to the Au NPs, which explains why the catalytic activity of the $Au@SiO_2/TiO_2$ samples is relatively lower than that of the $Au@TiO_2$ samples under UV light irradiation.

Degradation rate constants obtained by various Ag/TiO_2 and $Ag@SiO_2/TiO_2$ samples under the irradiation of UV light are also listed in Fig. 6. Overall, the Ag/TiO_2 samples show similar catalytic activities to the Au/TiO_2 samples. In contrast, the photocatalytic activities of the $Ag@SiO_2/TiO_2$ samples are much different from those of the $Au@SiO_2/TiO_2$. That is, the catalytic activities of $Ag@SiO_2/TiO_2$ were significantly higher than those of the Ag/TiO_2 samples. It can be deduced that this observation is closely related to the characteristic plasmonic absorption bands of Ag and $Ag@SiO_2$, located in the range of 410–440 nm, which is close to the UV region.

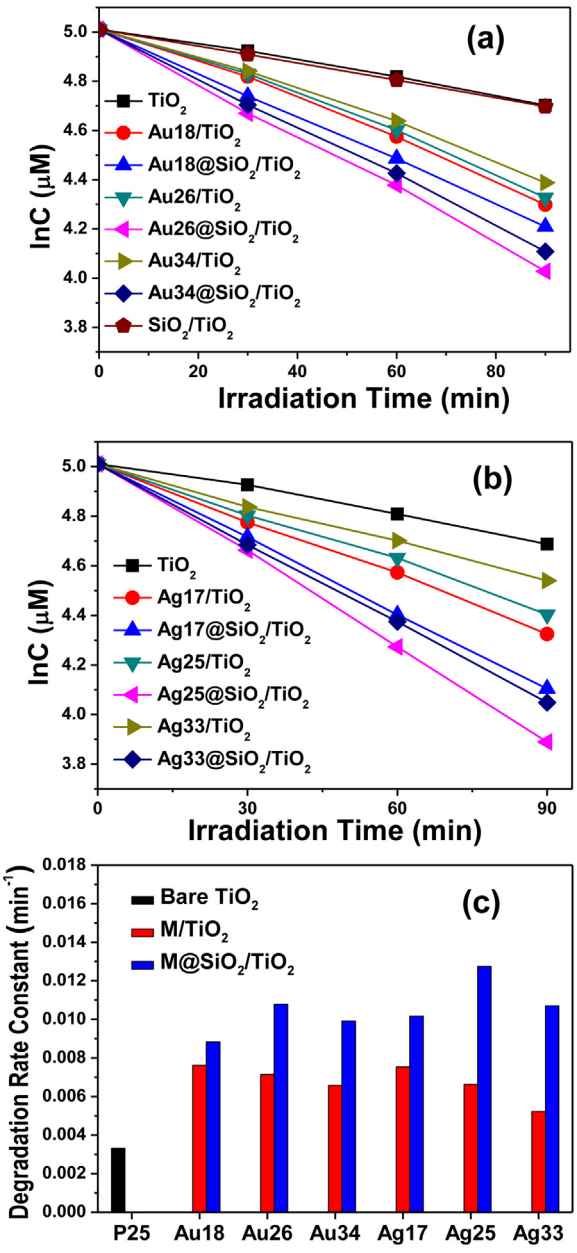

Fig. 7. Plots of $ln\,C$ vs. irradiation time for the photocatalytic decomposition of aqueous SA with the various Au/TiO_2 and $Au@SiO_2/TiO_2$ (a) and various Ag/TiO_2 and $Ag@SiO_2/TiO_2$ (b), and bar graphs for the degradation rate constants (k) of the bare TiO_2 and various plasmonic photocatalysts in decomposing aqueous SA (c). For all of the measurements, UV–vis light from a 300 W Xe-lamp equipped with an IR cut-off filter was applied.

Hence, the Ag or $Ag@SiO_2$ NPs could be activated significantly to generate the LSPR effect under UV light ($\lambda < 400$ nm) irradiation.

Second, the same photocatalytic measurements were also performed under UV–vis light irradiation. For the bare TiO_2, the photocatalytic activity was not altered by changing the light source, as seen in Fig. 7a. However, all of the Au/TiO_2 systems exhibited notably higher catalytic activities than the bare TiO_2, clearly indicating that the enhancement of the photocatalytic activity is due to the LSPR induced by the Au NPs, which are activated by the photons corresponding to their plasmonic absorption band. Interestingly, however, as the size of the Au NPs increased from 18 nm to 34 nm, their catalytic activity was slightly decreased, as seen in Fig. 7a. In contrast, the $Au@SiO_2$-loaded TiO_2 samples showed a much different trend in their catalytic activities. All of the $Au@SiO_2/TiO_2$

samples showed much higher photocatalytic activity than the corresponding Au/TiO_2 samples. In addition, as the size of the Au NPs increased from 18 nm to 26 nm, their catalytic activity was significantly enhanced, but further increasing the Au NP size to 34 nm slightly decreased their catalytic activity. As a control experiment, bare SiO_2 NP was loaded onto the TiO_2. It turned out that the loading of SiO_2 did not modify the catalytic activity of TiO_2, as shown in Fig. 7a, thus suggesting that the presence of SiO_2 on the TiO_2 surface does not affect the photocatalytic activity.

Photocatalytic decompositions of the aqueous SA with Ag/TiO_2 and Ag@SiO_2/TiO_2 systems under UV–vis light irradiation are shown in Fig. 7b. Basically, the photocatalytic activity trends of the Ag/TiO_2 and Ag@SiO_2/TiO_2 systems, depending on the size of the plasmonic NPs, are similar to those of the Au/TiO_2 and Au@SiO_2/TiO_2, respectively. That is, all of the Ag/TiO_2 samples exhibited much higher catalytic activities than the bare TiO_2. Moreover, as the size of the Ag NPs was increased from 17 nm to 33 nm, their catalytic activity was gradually decreased. Compared to the Ag/TiO_2, the Ag@SiO_2/TiO_2 samples exhibited quite different trend in their catalytic activities. All of the Ag@SiO_2/TiO_2 samples showed significantly higher photocatalytic activity than the corresponding Ag/TiO_2 samples. In addition, as the size of the Ag NPs increased from 17 nm to 25 nm, the catalytic activity of the Ag@SiO_2/TiO_2 samples was significantly enhanced, but further increasing their size to 33 nm leaded to a decrease of their photocatalytic activity, clearly indicating that Ag25@SiO_2 is the optimum size of the plasmonic NPs for photocatalytic applications.

Photocatalytic activities of the various plasmonic photocatalysts in decomposing SA under UV–vis light irradiation are summarized in the form of bar graphs, as shown in Fig. 7c. The Au and Ag loaded TiO_2 samples exhibit significantly higher catalytic activities than the bare TiO_2, but their activities gradually decrease as the sizes of the Au or Ag NPs increase. Noticeably, the photocatalytic activity of Ag/TiO_2 decreases more rapidly than that of Au/TiO_2, as the size of the NPs increases. Hence, the catalytic activity of Ag33/TiO_2 was relatively lower than that of Au34/TiO_2, although the Ag33 NP generates stronger LSPR than the Au34 NP.

Previously, the size-dependent photocatalytic activity for the Au/TiO_2 systems was explained by the Fermi level shift according to the size variation of Au NPs [12–14]. That is, as the size of Au NPs increases, their Fermi level shifts toward more positive side due to the quantum size effect. Thus the energy gap difference between the TiO_2 CB and Fermi level of Au NP is enlarged, leading to less efficient electron trapping by the Au NPs. However, the sizes of Au NPs and Ag NPs applied in this work are as large as 18–34 nm and 17–33 nm, respectively, which are too large to show an appreciable quantum size effect. Thus, the size-dependent photocatalytic activities of Au/TiO_2 and Ag/TiO_2 would not be caused by the Fermi level shift. We believe that the results obtained are more closely related to the LSPR sensitization effect. Under visible light irradiation, LSPR sensitization is known to be useful for photocatalytic oxidation reactions, because the holes generated in the noble metal NP and the electrons injected to the TiO_2 CB can participate in the oxidation reactions [23–32]. However, under UV–vis light irradiation, the contribution of the holes in the noble metal NPs will not be significant, because TiO_2 can also be excited and the holes in the TiO_2 VB have much stronger oxidation power than those in the noble metal NPs. Furthermore, there is a high possibility that the LSPR sensitization prevents the space-charge separation of the electron-hole pairs in TiO_2 (see Scheme 1a). As the size of the plasmonic NPs increases, the generated LSPR will increase, leading to the enhancement of local electric field. On one hand, this is favorable for the photocatalytic oxidation reactions, because more electron-hole pairs can be generated in TiO_2. On the other hand, due to the LSPR sensitization effect, the electron back transfer from the plasmonic NP to TiO_2 CB will also be increased, leading to a decrease of catalytic activity by interrupting the charge-separation in TiO_2.

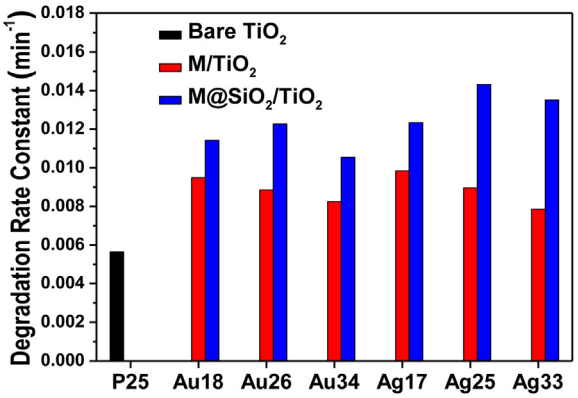

Fig. 8. Bar graphs for the degradation rate constants (k) of the bare TiO_2 and various plasmonic photocatalysts in decomposing aqueous aniline under UV–vis light.

The photocatalytic activities of several Au@SiO_2/TiO_2 and Ag@SiO_2/TiO_2 samples are also shown in Fig. 7c. The Ag@SiO_2/TiO_2 samples exhibit relatively higher photocatalytic activity than the Au@SiO_2/TiO_2 samples. For the silica-covered plasmonic NPs, the overall LSPR can be enhanced, but the LSPR sensitization effect is blocked due to the coverage of dielectric SiO_2 layer on the surface of the plasmonic NPs. Therefore, the major effect of the M@SiO_2 (M = Au or Ag) NPs on the catalytic performance of TiO_2 originates from the increase of local electric field near the plasmonic NPs. In this regard, the plasmonic NPs with stronger LSPR effect will induce higher photocatalytic performance, clearly explaining relatively higher catalytic activity of the Ag@SiO_2/TiO_2 systems than that of Au@SiO_2/TiO_2. We also monitored the size dependent plasmonic effect on the photocatalytic activity of the various Au@SiO_2/TiO_2 and Ag@SiO_2/TiO_2 samples. Among the various Au@SiO_2 and Ag@SiO_2 NPs, Au26 and Ag25 leaded to the highest photocatalytic activities. The result obtained implies that the LSPR reaches a maximum level at a size of 25–26 nm for both the Au@SiO_2 and Ag@SiO_2 NPs, thus implying that 25–26 nm is the optimum size for their application to plasmonic photocatalysts in decomposing organic compounds. In particular, Ag25@SiO_2/TiO_2 exhibits the highest efficiency in decomposing SA, with a degradation rate constant 3.8 times higher than that of the bare TiO_2.

We performed the same experiments for the decomposition of aqueous aniline under UV–vis light irradiation. Photocatalytic activities of the various Au/TiO_2, Au@SiO_2/TiO_2, Ag/TiO_2, and Ag@SiO_2/TiO_2 catalysts are compared in the bar graphs, as shown in Fig. 8. In addition, individual decomposition plots as a function of irradiation time are illustrated in Fig. S4. It was found that the obtained photocatalytic trends are compatible with those of SA decomposition. That is, the Ag@SiO_2/TiO_2 samples show relatively higher catalytic activities than the Au@SiO_2/TiO_2 samples and the 25 nm-sized plasmonic NPs is the optimum size for their application to the plasmonic photocatalysts. Resultantly, Ag25@SiO_2/TiO_2 exhibits the highest efficiency in decomposing aniline, with a degradation rate constant 2.5 times higher than that of the bare TiO_2.

As demonstrated in this work, the introduction of plasmonic NPs will be a promising strategy in designing highly efficient photocatalysts for decomposing organic pollutants.

4. Conclusions

A range of Au, Au@SiO_2, Ag and Au@SiO_2 NPs were selectively tailored, and loaded onto TiO_2 to obtain various plasmonic photocatalysts. In removing aqueous SA and aniline under UV–vis light

irradiation, both the Au/TiO_2 and Ag/TiO_2 showed significantly improved photocatalytic activity comparing with the bare TiO_2, but increasing the sizes of Au and Ag NPs induces a gradual decrease of catalytic activity. Although the Ag NPs show stronger LSPR effect than the Au NPs, the overall catalytic activity of the Ag/TiO_2 systems was not higher than Au/TiO_2, and the variation of their catalytic activities according to the size of the plasmonic NPs was more sensitive for Ag/TiO_2. The observed results seem to be due to the LSPR sensitization effect. In contrast, for the $Au@SiO_2/TiO_2$ and $Ag@SiO_2/TiO_2$ samples, the LSPR sensitization effect or the charge-separation role of the noble metals were blocked completely. Therefore, the local electric field enhancement will be the major effect. As a result, the plasmonic NPs with a stronger LSPR effect will induce a higher photocatalytic performance, clearly explaining the comparatively higher catalytic activity of the $Ag@SiO_2/TiO_2$ systems than that of $Au@SiO_2/TiO_2$. Particularly, $Ag25@SiO_2/TiO_2$ exhibits the highest catalytic activity in decomposing SA and aniline, which is evaluated to be 3.8 and 2.5 times, respectively, that of the bare TiO_2.

Acknowledgments

This work was supported by the National Research Foundation of Korea (NRF) (NRF-2015R1D1A1A01057390) and the Korea Center for Artificial Photosynthesis (KCAP) funded by the Ministry of Science, ICT and Future Planning through the NRF (No. 20090093886).

Appendix A. Supplementary data

Supplementary data associated with this article can be found, in the online version, at http://dx.doi.org/10.1016/j.apcatb.2017.05.025.

References

[1] A. Fujishima, K. Honda, Nature 238 (1972) 37–38.
[2] P. Wang, B. Huang, Y. Daia, M.-H. Whangbo, Phys. Chem. Chem. Phys. 14 (2012) 9813–9825.
[3] G.C. Bond, P.A. Sermon, G. Webb, D.A. Buchanan, P.B. Wells, J. Chem. Soc. Chem. Commun. (1973) 444–445.
[4] Y.M. Gao, W. Lee, R. Trehan, R. Kershaw, K. Dwight, A. Wold, Mater. Res. Bull. 26 (1991) 1247.
[5] W. Lee, H.S. Shen, K. Dwight, A. Wold, J. Solid State Chem. 106 (1993) 288–294.
[6] K. Awazu, M. Fujimaki, C. Rockstuhl, J. Tominaga, H. Murakami, Y. Ohki, N. Yoshida, T. Watanabe, J. Am. Chem. Soc. 130 (2008) 1676–1680.
[7] C. Zhang, H. He, Catal. Today 126 (2007) 345–350.
[8] C. Zhang, H. He, K.-I. Tanaka, Appl. Catal. B 65 (2006) 37–43.
[9] A. Naldoni, M. D'Arienzo, M. Altomare, M. Marelli, R. Scotti, F. Morazzoni, E. Selli, V.D. Santo, Appl. Catal. B 130–131 (2013) 239–248.
[10] D. Behar, J. Rabani, J. Phys. Chem. B 110 (17) (2006) 8750–8755.
[11] S. Scirè, S. Minicò, C. Crisafulli, C. Satriano, A. Pistone, Appl. Catal. B 40 (2003) 43–49.
[12] V. Subramanian, E.E. Wolf, P.V. Kamat, J. Am. Chem. Soc. 126 (2004) 4943–4950.
[13] Y. Tian, T. Tetsu, J. Am. Chem. Soc. 127 (2005) 7632–7637.
[14] M. Jakob, H. Levanon, P.V. Kamat, Nano Lett. 3 (2003) 353–358.
[15] T. Hirakawa, P.V. Kamat, J. Am. Chem. Soc. 127 (2005) 3928–3934.
[16] R.-S. Sonawane, M.-K. Dongare, J. Mol. Catal. A 43 (2006) 68–76.
[17] S. Linic, P. Christopher, D.B. Ingram, Nat. Mater. 10 (2011) 911–921.
[18] J.-J. Chen, J.C.S. Wu, P.C. Wu, D.P. Tsai, J. Phys. Chem. C 115 (2011) 210–216.
[19] H. Zhang, X.F. Fan, X. Quan, S. Chen, H.T. Yu, Environ. Sci. Technol. 45 (2011) 5731–5736.
[20] X. Shi, K. Ueno, N. Takabayashi, H. Misawa, J. Phys. Chem. C 117 (2013) 2494–2499.
[21] E. Dulkeith, T. Niedereichholz, T.A. Klar, J. Feldmann, G. Von Plessen, D.I. Gittins, K.S. Mayya, F. Caruso, Phys. Rev. B 70 (2004) 205424–205427.
[22] D.M. Schaadt, B. Feng, E.T. Yu, Appl. Phys. Lett. 86 (2005) (063106/1-063106/3).
[23] X. Zhang, Y.L. Chen, R.-S. Liu, D.P. Tsai, Rep. Prog. Phys. 76 (2013) 046401.
[24] S. Link, M.A. El-Sayed, J. Phys. Chem. B 103 (1999) 8410–8426.
[25] Y. Tian, T. Tatsuma, J. Am. Chem. Soc. 127 (2005) 7632–7637.
[26] Z. Zheng, B. Huang, X. Qin, X. Zhang, Y. Dai, M.-H. Whangbo, J. Mater. Chem. 21 (2011) 9079–9087.
[27] E. Kowalska, H. Remita, C. Colbeau-Justin, J. Hupka, J. Belloni, J. Phys. Chem. C 112 (2008) 1124–1131.
[28] I.M. Arabatzis, T. Stergiopoulos, D. Andreeva, S. Kitova, S.G. Neophytides, P. Falaras, J. Catal. 220 (2003) 127–135.
[29] C.K. Sun, F. Vallee, L.H. Acioli, E.P. Ippen, J.G. Fujimoto, Phys. Rev. B 50 (1994) 15337–153548.
[30] S.M. Yoo, S.B. Rawal, J.E. Lee, J. Kim, H.-Y. Ryu, D.-W. Park, W.I. Lee, Appl. Catal. A 499 (2015) 47–54.
[31] T. Jiang, C. Jia, L. Zhang, S. He, Y. Sang, H. Li, Y. Li, X. Xu, H. Liu, Nanoscale 7 (2015) 209–217.
[32] C.K. Song, J. Baek, T.Y. Kim, S. Yu, J.W. Han, J. Yi, Appl. Catal. B 198 (2016) 91–99.
[33] X. Zhou, G. Liu, J. Yu, W. Fan, J. Mater. Chem. 22 (2012) 21337–21354.
[34] M.R. Elahifard, S. Rahimnejad, S. Haghighi, M.R. Gholami, J. Am. Chem. Soc. 129 (2007) 9552–9553.
[35] P. Christopher, H. Xin, S. Linic, Nat. Chem. 3 (2011) 467–472.
[36] A. Tanaka, S. Sakaguchi, K. Hashimoto, H. Kominami, ACS Catal. 3 (2013) 79–85.
[37] E. Kowalska, R. Abea, B. Ohtani, Chem. Commun. (2009) 241–243.
[38] S. Link, M.A. El-Sayed, Int. Rev. Phys. Chem. 19 (2000) 409–453.
[39] K. Mori, M. Kawashima, M. Che, H. Yamashita, Angew. Chem. Int. Ed. 49 (2010) 8598–8601.
[40] P. Christopher, D.B. Ingram, S. Linic, J. Phys. Chem. C 114 (2010) 9173–9177.
[41] S.G. Kumar, L.G. Devi, J. Phys. Chem. A 115 (2011) 13211–13241.
[42] S. Hu, F. Li, Z. Fan, Bull. Korean Chem. Soc. 34 (2013) 3671–3676.
[43] K. Hashimoto, H. Irie, A. Fujishima, Jpn. J. Appl. Phys. 44 (2005) 8269–8285.
[44] B.R. Cuenya, Thin Solid Films 518 (2010) 3127–3150.
[45] S. Bera, J.E. Lee, S.B. Rawal, W.I. Lee, Appl. Catal. B 199 (2016) 55–63.
[46] X. Zhang, Y. Zhu, X. Yang, S. Wang, J. Shen, B. Lin, C. Li, Nanoscale 5 (2013) 3359–3366.
[47] J.-J. Chen, J.C.S. Wu, P.C. Wu, D.P. Tsai, J. Phys. Chem. C 116 (2012) 26535–26542.
[48] J. Xu, X. Xiao, A.L. Stepanov, F. Ren, W. Wu, G. Cai, S. Zhang, Z. Dai, F. Mei, C. Jiang, Nanoscale Res. Lett. 81 (2013) (73/1-73/73).
[49] M.K. Kumar, S. Krishnamoorthy, L.K. Tan, S.Y. Chiam, S. Tripathy, H. Gao, ACS Catal. 1 (2011) 300–308.
[50] M.E. Stewart, C.R. Anderton, L.B. Thompson, J. Maria, S.K. Gray, J.A. Rogers, R.G. Nuzzo, Chem. Rev. 108 (108) (2008) 494–521.
[51] R. Kaur, B. Pal, New J. Chem. 39 (2015) 5966–5976.
[52] J. Turkevich, P.C. Stevenson, J. Hillier, Discuss. Faraday Soc. 11 (1951) 55–75.
[53] G. Frens, Nat. Phys. Sci. 241 (1973) 20–21.
[54] J. Kimling, M. Maier, B. Okenve, V. Kotaidis, H. Ballot, A. Plech, J. Phys. Chem. B 110 (2006) 15700–15707.
[55] W. Stöber, A. Fink, E. Bohn, J. Colloid Interface Sci. 26 (1968) 62–69.
[56] Y. Lu, Y. Yin, Z.-Y. Li, Y. Xia, Nano Lett. 2 (2002) 785–788.
[57] C.D. Sanguesa, R.H. Urbina, M. Figlarz, J. Solid State Chem. 100 (1992) 272–280.
[58] D.J. Kim, S.H. Jeong, J.H. Moon, Nanotechnol 17 (2006) 4019–4024.
[59] N.G. Bastuís, F. Merkoci, J. Piella, V. Puntes, Chem. Mater. 26 (2014) 2836–2846.
[60] C. Graf, D.L.J. Vossen, A. Imhof, A. van Blaaderen, Langmuir 19 (2013) 6693–6700.
[61] J. Asselin, P. Legros, A. Grégoire, D. Boudreau, Plasmonics 11 (2016) 1369–1376.
[62] Z. Bai, R. Chen, P. Si, Y. Huang, H. Sun, D.-H. Kim, ACS Appl. Mater. Interfaces 5 (2013) 5856–5860.
[63] J. Yang, F. Zhang, Y. Chen, S. Qian, P. Hu, W. Li, Y. Deng, Y. Fang, L. Han, M. Luqman, D. Zhao, Chem. Commun. 47 (2011) 11618–11620.
[64] J. Zhou, F. Ren, S. Zhang, W. Wu, X. Xiao, Y. Liu, C. Jiang, J. Mater. Chem. A 1 (2013) 13128–13138.